Structural distortions in 5–10 nm silver nanoparticles under high pressure

K. J. Koski and N. M. Kamp

Department of Chemistry, University of California–Berkeley, Berkeley, California 94720, USA

R. K. Smith

Materials Science Division, Lawrence Berkeley National Laboratory, Berkeley, California 94720, USA

M. Kunz and J. K. Knight

Advanced Light Source, Lawrence Berkeley National Laboratory, Berkeley, California 94720, USA

A. P. Alivisatos[*]

Department of Chemistry, University of California–Berkeley, Berkeley, California 94720, USA
and Materials Science Division, Lawrence Berkeley National Laboratory, Berkeley, California 94720, USA

We present experimental evidence that silver nanoparticles in the size range of 5–10 nm undergo a reversible structural transformation under hydrostatic pressures up to 10 GPa. We have used x-ray diffraction with a synchrotron light source to investigate pressure-dependent and size-dependent trends in the crystal structure of silver nanoparticles in a hydrostatic medium compressed in a diamond-anvil cell. Results suggest a reversible linear pressure-dependent rhombohedral distortion which has not been previously observed in bulk silver. We propose a mechanism for this transition that considers the bond-length distribution in idealized multiply twinned icosahedral particles. To further support this hypothesis, we also show that similar measurements of single-crystal platinum nanoparticles reveal no such distortions.

I. INTRODUCTION

Noble metal nanoparticles, such as Ag, Cu, Pd, and Au, at sizes of <10 nm often possess multiply twinned grains that allow them to adopt shapes and atomic structures not existing in bulk materials.[1,2] The properties exhibited by particles with multiply twinned polycrystalline structures are often far different from those of single-crystalline particles or from the bulk. The exposure of specific surfaces and the presence of particular grain boundaries facilitate interesting mechanical and chemical behaviors and alter the surface properties.[1,3,4] The argument has been made that these crystal structures are adopted by clusters because the energy cost of the internal strain is offset by a favorable rearrangement of surface atoms.[5] The question then arises, what happens to the internal strain and the atomic structure if one puts an external stress, such as pressure, onto these types of structures?

These intermediate-sized clusters frequently feature fivefold twin junctions which yield structures that are ideally described as decahedral (Dh) or icosahedral (Ih).[2,6] The Dh and Ih are constructed of irregular tetrahedral grains that have body-centered orthorhombic and rhombohedral crystal symmetries, respectively. The corresponding orthorhombic and rhombohedral distortions of the fcc lattice introduce small but uniform strains within each tetrahedral grain.[7,8] Reinhard et al.[5] also noted that icosahedral structures in Ni, Ar, Cu, Au, Pb, and Ag have the general feature that the strain within each tetrahedron is nonuniform giving rise to a convex deformation of the outer facets. Since these structures are intrinsically strained, addition of pressure should alter the relative energetics of strain and surface energies which could have a large impact in the structural behavior of these particles.

The present study focuses on silver nanoparticles in the intermediate-size range of 5–10 nm, which have been shown to possess an icosahedral structure in both free and substrate-supported cases. Silver supported on a substrate was investigated using scanning tunneling microscopy by Silly et al.[9] and was shown to adopt an icosahedral form. Similar structures were observed in unsupported silver clusters produced by an inert gas aggregation source and measured with electron diffraction.[5,10] Recent experimental measurements by Xing et al.[10] of small clusters of <100 atoms showed size-dependent fivefold symmetry which evolved to icosahedral symmetry with increasing size. Hall et al.[11] experimentally observed for larger clusters from 2–4 nm a mixture of icosahedral, decahedral, and fcc structures. More importantly, Reinhard et al.[5] showed a mixture of icosahedral and fcc structures for particles between 4 and 11 nm.

Bulk silver adopts the face-centered cubic structure. Under pressure, no phase transitions or distortions have yet been identified up to 200 GPa using shock compression methods[12] and up to 146 GPa using diamond-anvil cell (DAC) compression techniques.[13] More recently, 10 nm commercially available Ag nanoparticles were studied up to pressures of 30 GPa by Gu et al.[14] No phase transitions or noncubic distortions were observed in these experiments; however, a higher bulk modulus than that of bulk silver was noted.

Here we present experimental evidence that silver nanoparticles in the intermediate-size range of 5–10 nm in multiply twinned structures undergo a structural distortion consistent with a rhombohedral distortion with increasing pressure. Transmission electron micrographs of these particles show a mixture of morphologies including multiply twinned icosahedral structures. We propose a mechanism for this distortion

based on the crystallographic structure and grain boundaries of these particles. This hypothesis is consistent with a control experiment. We find that similar measurements on single-crystal fcc nanoparticles of platinum show no such distortion, which suggests that the grain boundaries are essential to the phenomenon.

II. EXPERIMENT

A. Nanoparticle synthesis and characterization

Silver nanoparticles were synthesized via polyol reduction of silver perchlorate in refluxing toluene with oleylamine and oleic acid as surfactants. Silver perchlorate (97%), 1,2-hexadecanediol (90%), oleylamine (70%), oleic acid (99%), ethylcyclohexane (99%), toluene, hexane, 2-propanol, pentane, and isopentane were purchased from Sigma Aldrich (St. Louis, MO) and used as received. All solvents used were anhydrous and stored under inert atmosphere. All syntheses were performed under air-free conditions.

In a typical synthesis, 0.5 mmol 1,2-hexadecanediol was added to a round bottom flask fitted with a condenser, thermocouple adapter, and a magnetic stir bar and was evacuated and backfilled with argon. Oleylamine (0.6 mmol) mixed with 9.8 mL toluene was added to the reaction flask with vigorous stirring and brought to reflux at 110 °C. Once at reflux, 0.25 mmol $AgClO_4$ dissolved in 0.2 mL toluene was rapidly injected into the flask. Formation of nanoparticles occurred instantly upon mixing and was indicated by the originally colorless solution turning dark brown. After 2 min, 0.1 mL oleic acid was injected and the mixture was cooled to room temperature. The particles were cleaned under air-free conditions by precipitation with three volume equivalents of 2-propanol and centrifugation (4000 rpm for 5 min). Nanoparticles were resuspended in either toluene, hexane, or pressure-transmitting fluid (1:1 v/v pentane:isopentane or ethylcyclohexane). The average nanoparticle diameter was controlled by varying the time for particle ripening before the injection of the oleic acid up to a maximum of 24 h. Oleic acid binds to the particle surface more tightly than oleylamine does, thus, it increases particle stability and prevents growth at these temperatures.[15,16] Oleylamine likely serves dual purposes in this synthesis: (i) as an addition reducing agent and (ii) to act as a surfactant and control growth of nanocrystals in solution.[17]

Platinum nanoparticles of 2.8 ± 0.8 nm used in these experiments were synthesized by the polyol method of Sobal *et al.*[18] that is similar to the one outlined for Ag here. Transmission electron microscopy (TEM) measurements of these particles showed that they did not possess multiply twinned structures and were indeed single-crystal fcc nanoparticles.

The particle size was estimated by counting particles ($n > 3000$) with TEM using a 200 kV Technai G^2 20. The samples used were synthesized from one month to one day in advance of the high-pressure experiments and were stored cold in 1:1 pentane:isopentane, hexane, or toluene under an argon atmosphere in a refrigerator to prevent aggregation and degradation. The particle sizes were reaffirmed with TEM immediately before experimental x-ray diffraction (XRD) measurements.
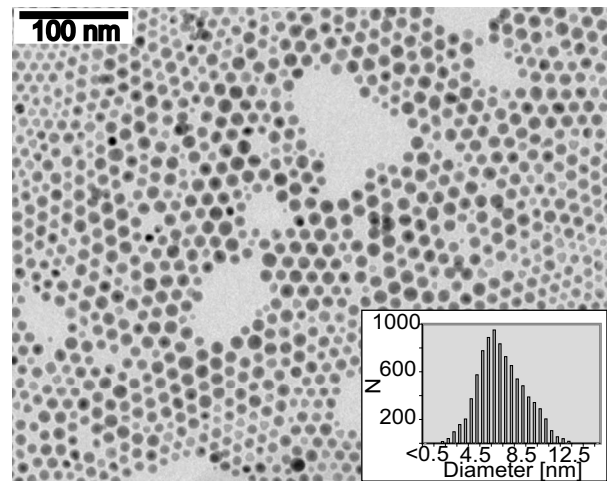

FIG. 1. TEM of the 7.2 nm silver sample used in the x-ray diffraction. Histogram of nanoparticle size distribution is shown in the inset.

Figure 1 shows a representative TEM image and histogram of nanoparticle diameter of a sample of silver nanoparticles used in this study. This particular sample had particles of diameter 7.2 ± 1.7 nm and is typical of the structure and size distribution of nanoparticles used in these experiments. The contrast variations in individual particles in this image are apparent indicating polycrystalline particles. There appears to be a mixture of particle morphologies showing that the particles are not spherical. This synthesis yields a mostly narrow size distribution.

Figure 2 shows a selection of high-resolution TEM images of the silver nanoparticles synthesized for these experiments. As predicted in the literature for the sizes of silver nanoparticles used in this study, the silver nanoparticles tended to be primarily multiply twinned particles approximating the idealized icosahedral structure.[5,19] Also observed are occasional single-crystal silver nanoparticles as shown in the center of this figure. Predominantly, though, we observed multiply twinned structures possessing twin pentajunctions.

All silver nanoparticle sizes and distributions presented in this study are shown in Table I. Particles shown with an asterisk were solvated in pressure-transmitting fluids that were not stored in inert atmosphere and were loaded in air.
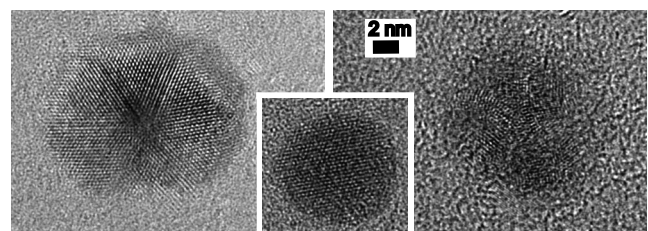

FIG. 2. Representative high-resolution TEM images of silver nanoparticles used in the x-ray diffraction experiments. The samples used in this study primarily possessed multiply twinned domains (left and right images); however, single-crystal particles were occasionally observed (center image).

TABLE I. Table of silver and platinum nanoparticles' sizes and distributions used in this study. Asterisks indicate samples exposed to oxygen during sample loading.

	Mean diameter (nm)	σ (nm)
Ag	5.0	1.6
	2.6	1.2*
	7.2	1.7
	9.4	4.0*
	9.8	2.5
	10.0	3.0
Pt	2.8	0.8

B. High-pressure x-ray diffraction measurements

High-pressure x-ray diffraction measurements were acquired on beamline 12.2.2 of the Advanced Light Source using an energy of 20 keV ($\lambda = 0.6199$ Å).[20] The beam size was 50×50 μm. Patterns were acquired using a Mar-345 image plate. Typical acquisition times were between 15 and 20 min.

The sample was loaded in a DAC and centered relative to the x-ray beam vertically and horizontally on a rotation axis. The recentering procedure was performed whenever the diamond cell was removed or remounted. Since the cell was removed to increase and to measure the pressure, this was repeated for every pressure step. In order to decrease signal from background air scattering, a small beamstop (second to one immediately before the detector) was placed behind the DAC.

The sample-to-detector distance and detector tilt were calibrated with a LaB$_6$ (NIST) standard. All two-dimensional (2D) XRD images were integrated to one-dimensional (1D) patterns using FIT2D,[21] using a mask to exclude the two beamstops and single-crystal ruby diffraction spots from ruby loaded into the cell for pressure calibration (see later text).

A gas membrane-driven diamond-anvil cell (Diacell, Easylab, U.K.) with 400 μm diamond culets was used for high-pressure measurements. Spring-steel gaskets were preindented to 85 μm thickness and a centered 200-μm-diameter gasket hole was drilled with an electrical discharge machine (EDM). Several grains of annealed ruby were placed into the gasket hole to measure the pressure inside of the diamond cell.

Sample preparations were as specified throughout the text. Two preparations were used: one that allowed for the possibility of sample oxidation and the other intended to prevent oxidation of the sample.

The sample was loaded in a 1:1 by volume pentane:isopentane mixture under an argon atmosphere in a glove box. A 1:1 V/V mixture of pentane:isopentane is hydrostatic up to 7 GPa, and it was used as the pressure-transmitting fluid because of its hydrostatic nature.[22,23] Additionally, silver nanoparticles not exposed to air are readily soluble in 1:1 pentane:isopentane unlike other pressure-transmitting fluids such as 4:1 methanol:ethanol. Alternatively, the sample was loaded in ethylcyclohexane under air. Ag nanoparticles exposed to air tended to precipitate from solution in 1:1 pentane:isopentane. The degree of hydrostaticity of ethylcyclohexane is unknown, but it has been the choice quasihydrostatic solvent of several high-pressure experiments including those performed on nanoparticles.[24–26]

The sample was loaded to be sufficiently concentrated so as to give an adequate diffraction signal but still be visually transparent both in solution and in the diamond-anvil cell. The solution color in the DAC was a light yellow to a light red color. If the solution of nanoparticles in the DAC was either opaque or a dark red color, or if visible aggregates formed, the cell was reloaded. Avoiding agglomeration is important to differentiate nanoscale effects from particle interaction effects at high pressures. No gasket deformation was noticed during this study.

C. Pressure determination

The pressure in the diamond cell was determined using the pressure-dependent ruby fluorescence method.[27,28] Three to five pieces of annealed ruby grains in the cell were used for measurements of the pressure. Values of the wavelengths (λ) of the R_1 and R_2 fluorescence emissions were obtained from the fit of two Lorentzian peaks to the fluorescence spectra. The pressure was determined by the relation $P = (\lambda - \lambda_{ambient})/0.365$ as in Ref. 27. The ambient values ($\lambda_{ambient}$) of R_1 and R_2 were measured by a single grain of annealed ruby placed on a microscope slide. The final pressure was determined by the average of the results for the R_1 and R_2 peaks. Spread in the pressure was calculated by the standard deviation of the results for all ruby peaks per each pressure measurement. The typical spread of pressures, below the pressure-transmitting fluid glass transition, was on the order of <0.1 GPa. The degree of hydrostaticity was checked via the full width at half maximum of the fluorescence peaks and by the distribution of pressures across the cell. Throughout the experiment great care was taken to maintain the temperature of the DAC for both ruby and XRD measurements at $27-28$ °C.

D. Data analysis

A background diffraction pattern was acquired after each pressure run with the diamond cell filled only with the pressure medium and a few grains of ruby. This pattern, in 1D format, was subtracted from each data set after it was scaled to match the integrated intensity and decay of the electron current in the storage ring. To determine the position and width, each peak in each XRD curve was fit with a Lorentzian peak using MATHEMATICA.

III. RESULTS

A. Silver nanoparticles

Selected x-ray diffraction data versus pressure for silver nanoparticles of 9.4 ± 2.7 nm loaded in ethylcyclohexane are shown in Fig. 3. It is interesting to note that the relative shifts of the {111} and the {200} peaks are not the same with pressure.
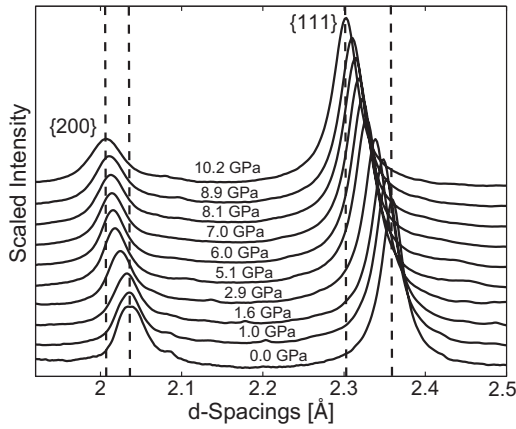
FIG. 3. Stacked plot of the x-ray diffraction patterns of 9.4 nm silver nanoparticles compressed in a DAC from 0 to 10 GPa. The relative shifts of the {111} and the {200} peaks are not the same with pressure. Dashed lines are drawn as guides for the eyes.

Figure 4 shows the ratio of the *d* spacings of the {200} to the {111} diffraction positions of a 7.2 ± 1.7 nm sample of silver nanoparticles. Since bulk silver metal adopts a fcc crystal structure up to a hydrostatic pressure of 150 GPa, each of the lattice directions in the cubic structure should compress isotropically. In a cubic crystal, the ratio of the {200} peaks to the {111} peaks should be $\sqrt{3/4} = 0.866$ and should stay constant with increasing pressure. We observe a distinct linear increase in the ratio of the *d* spacings with increasing pressure. Upon decompression, decreasing pressure points return along the same linear trend. In measurements where sample loss from the DAC with decreasing pressure is small, we observe full reversal of the distortion. This plot clearly demonstrates the noncubic behavior of silver nanoparticles as a function of pressure.

In Fig. 5, we show how the *d* spacings of the {111}, {200}, and {220} peaks for several sizes of silver nanoparticles change as a function of applied pressure. Figure 5(A) shows
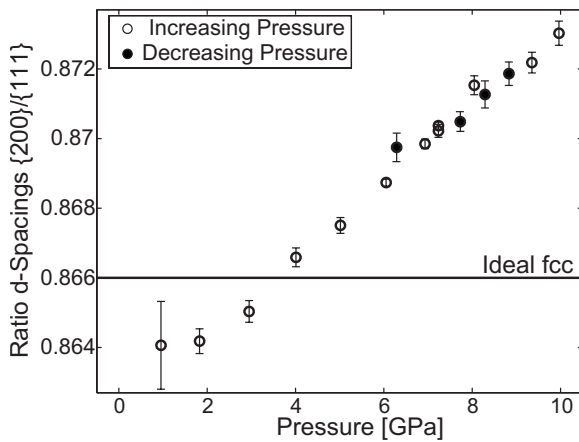

FIG. 4. Plot of the ratio of the *d* spacings of the {200} peak to the {111} peak. This silver nanoparticle sample was 7.2 nm in diameter and was loaded in 1:1 pentane:isopentane under an argon atmosphere. Solid line corresponds to the ratio of an ideal fcc structure (0.866). This plot clearly demonstrates noncubic distortion with increasing pressure.
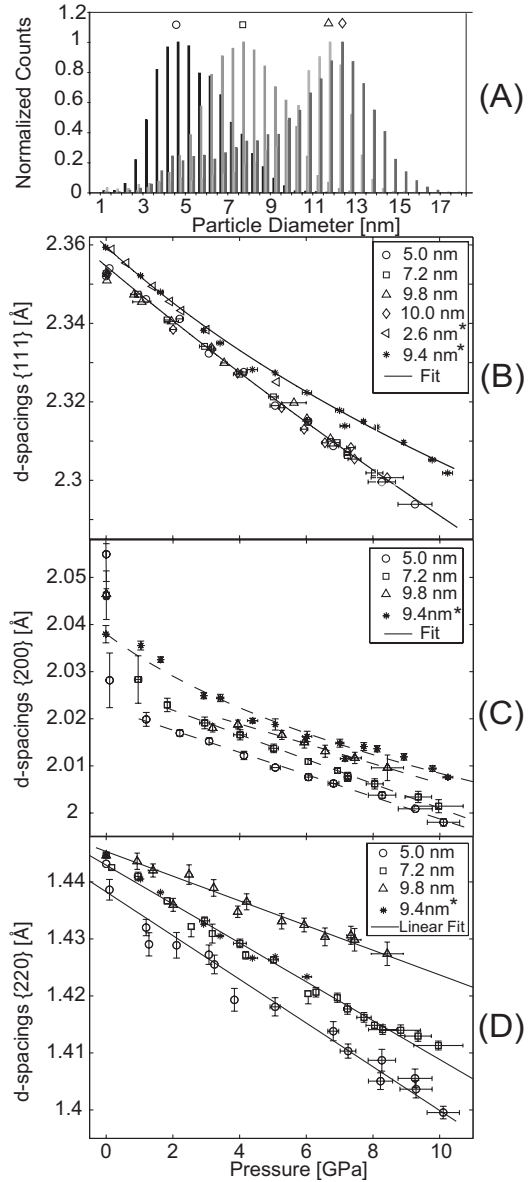

FIG. 5. *d* spacings as a function of measured pressure. (A) Shows a histogram of nanoparticle sizes of the Ag samples not exposed to oxygen. (B), (C), and (D) are plots of the {111}, {200}, and {220} *d* spacings with pressure, respectively. Lines are drawn on (B), (C), and (D) as guides for the eyes. Samples labeled with an * were exposed to oxygen during sample loading.

a histogram of the diameter of the different particles used in this experiment loaded in 1:1 V/V pentane:isopentane to fully demonstrate the size dependence of the noncubic distortion. In the plots, the * particles are those that have been exposed to oxygen postsynthesis. All other particles were prepared in an oxygen-free environment and loaded in the DAC in an argon atmosphere.

Figure 5(B) shows that for all sizes of Ag nanoparticles not exposed to oxygen, the compression of the {111} planes is, surprisingly, size independent. Particles exposed to oxygen show a similar trend also independent of particle size but shifted to larger *d* spacings. Figures 5(A) and 5(B) show, respectively, that the size dependence and distortion behavior
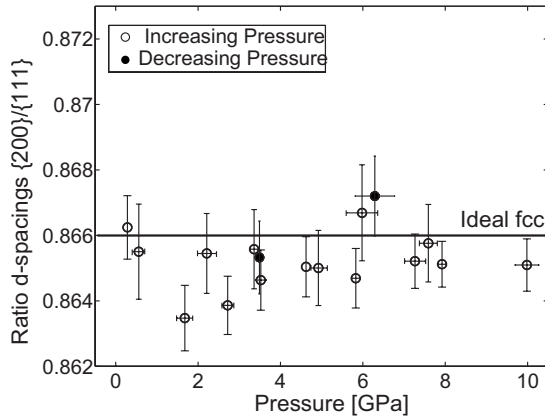
FIG. 6. Ratio of the *d* spacings of the {200} to the {111} x-ray diffraction peaks in 3 nm platinum nanoparticles. A solid line is drawn at the *d*-spacing ratio for an ideal fcc structure. The plot demonstrates little deviation from cubic structure.

are more apparent in the {220} and {200} planes. These plots show that there is size-dependent compression with increasing pressure that differs among the diffraction planes. Because of peak overlaps, the curve fits to obtain d_{200} were poorly behaved below 2 GPa so that these values may not be as accurate. The {220} peak demonstrates a linear pressure-dependent behavior that strongly depends on size. The amount of compression is less for larger particles along this direction.

As a guide for the eye, linear fits are made to the *d* spacings of the {220} reflection. For the {200} *d* spacings, a parabolic dashed line is drawn for the 9.4 nm particles and linear dashed trend lines are drawn for all other particles. For the {111}, with the small error bars and the small curvature, a similar trend line is drawn but generated with a fit of a Vinet equation.[29] The Vinet equation is a convenient and reasonable curve to fit this data. However, since these reflections do not behave as they would in the cubic materials, this fit has no physical meaning beyond a trend line.

B. Platinum fcc nanoparticles

We performed control experiments with single-crystal fcc platinum nanoparticles in order to test whether the observed structural distortions in silver multiply twinned particles might (1) be an artifact of the measurement and/or data analysis methods or (2) appear in nontwinned particles, which would cast doubt on our results and proposed mechanism.

These particles were synthesized as described earlier; TEM measurements of these particles showed that they did not possess multiply twinned structures and were indeed single-crystal fcc nanoparticles. Figure 6 presents the ratio of the $d_{\{200\}}/d_{\{111\}}$ from experimental x-ray diffraction peaks of platinum nanoparticles as a function of pressure. The data do not show the same noncubic distortion trend with pressure as was observed for Ag nanoparticles. The axes of this plot have been given the same scale as that of Fig. 4 to demonstrate the magnitude of this effect. Within the error of our

measurements, platinum retains its cubic crystal structure with pressure.

IV. DISCUSSION

Silver in the bulk adopts a fcc crystal structure at ambient conditions. Under increasing hydrostatic pressure, each of the lattice directions in the cubic structure should compress isotropically unless there is a driving nonhydrostaticity or a similar mechanism that causes the structure to deform anisotropically. This derives directly from the cubic symmetry; observation of something else indicates that something must be breaking that symmetry. Such a symmetry-breaking mechanism is the presence of twin pentajunctions that construct the ideally icosahedral morphology of intermediate-size silver nanoclusters.

For the two lower-symmetry structures (decahedra and icosahedra) that are the dominant idealized shapes of silver nanoparticles of this size range, two types of distortion are consistent: orthorhombic (decahedral particles) or rhombohedral (icosahedral particles).[7] In an orthorhombic distortion, the {111} peak from an undistorted fcc structure splits into two equal intensity peaks, the {200} separates into two peaks with one twice as intense as the other, and the {220} peak splits into three peaks with one four times as intense as the other two. This is accompanied by a concomitant shift of the *d* spacings.[7] In a rhombohedral distortion, a different scenario occurs with the {111} peak separating into two peaks with one a third the intensity of the other. The {200} peak remains unchanged, and the {220} peak splits into a doublet of equal intensity.[7] In our experiments, we more likely assign a rhombohedral distortion because (1) we see the {111} peak broaden possibly with the addition of a shoulder whereas it would be unchanged in an orthorhombic distortion and (2) we observe no change in width to the {200} peak which would become a doublet in an orthorhombic distortion. This hypothesis is consistent with multiply twinned particles possessing icosahedral symmetry.

There are several scenarios that are potentially responsible for the noncubic distortion observed in Ag nanoparticles beyond that of the multiply twinned nature of the particles. These are: (i) a pressure-dependent deformation consistent with the elastic constants, (ii) the presence of an oxide layer on the particles, and (iii) nonhydrostatic conditions. Ruling out these possibilities is addressed here.

A. Elastic constants

We first consider that the stress may be nonhydrostatic and that an ensemble of randomly oriented particles may show an average deviation from cubic symmetry simply because some crystal directions are more compressible than others. If a bulk crystal deforms under a nonhydrostatic stress, the directionally dependent Young's moduli provide a good estimator of which direction the lattice will preferentially compress. The lattice directions with the smaller value of a directional Young's modulus will compress more.

The elastic constants, primarily the compliances, of bulk silver have been measured by several sources[30–35]—the most

TABLE II. Directionally dependent Young's moduli in GPa calculated from compliances of Ref. 35.

Ag	$E\langle 111 \rangle$ (GPa)	$E\langle 100 \rangle$ (GPa)	$E\langle 110 \rangle$ (GPa)
	121.4	42.94	83.33

recent by Wolfenden *et al.*[35] Using the expressions for calculating the Young's modulus, *E*, outlined in Nye,[36] Wolfenden's measurements can be presented in terms of directional Young's moduli as shown in Table II.

This table illustrates that in bulk silver, the directionally dependent Young's modulus, *E*, is greater in the $\langle 111 \rangle$ than in the $\langle 200 \rangle$ and $\langle 220 \rangle$ directions ($E\langle 111 \rangle > E\langle 110 \rangle > E\langle 100 \rangle$). If the silver nanoparticles behaved like the bulk material, this would mean that the nanoparticles would more likely compress in the {200} direction than the {111} direction. For Ag nanoparticles we observe more compression along the {111} direction than the {200} direction, indicating that the observed distortion is unlikely to be caused by an interaction between nonhydrostaticity and elastic anisotropy.

B. Surface oxidation

Much of the effect of oxygen on the surface on nanoparticles is still not understood. It is known that thin silver films readily oxidize forming AgO and Ag_2O.[37] In some noble nanoparticle cases, indications are that it alters metal-metal bond lengths.[38] It is unclear what the effects of a surface oxide layer would be on these particular nanoparticles of silver. Detecting an appreciable surface oxide layer is also difficult since a monolayer or two of silver oxide will not possess a strong enough diffraction peak to render it visible in x-ray diffraction patterns or in electron diffraction.

In this study, to show that a surface oxide layer was not responsible for the observed distortion, we measured both particles that had been exposed to air and those loaded in inert conditions. Figure 3 presented a stacked plot of 9.4 nm Ag nanoparticles that had been loaded in air and in solvents not stored under inert conditions. A plot of the ratios of the *d* spacings for particles exposed to air also show noncubic behavior. As a comparison, Fig. 7 shows a stacked plot of 7.2 ± 1.7 nm silver nanoparticles loaded under an inert atmosphere. A plot of the ratios of the *d* spacings for this data showing noncubic behavior is seen in Fig. 4. The strong {111} reflections compress more than the {200} and {220} *d* spacings.

In both samples exposed to air and those not exposed, a noncubic distortion of similar magnitude is observed. Therefore, the existence of an oxide layer is not entirely responsible for the noncubic distortion. However, as noted throughout the text, the oxide layer does indeed affect the behavior of the distortion in a quantifiable manner. It appears to have the effect of dampening the magnitude of the distortion and it gives rise to a relative shift of the *d* spacings from those particles not exposed to air during loading, preparation, and experimentation.
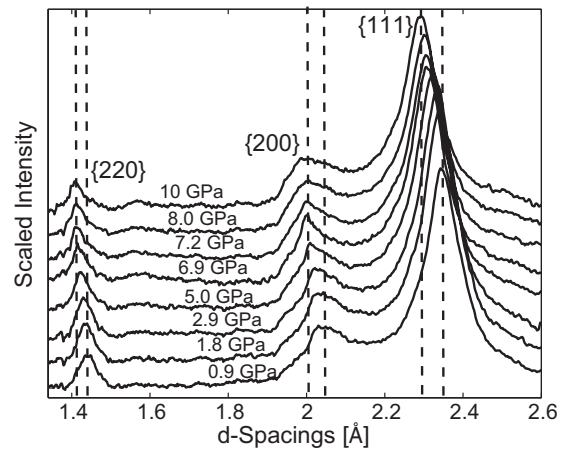

FIG. 7. Stacked plot of the x-ray diffraction data of silver as a function of pressure clearly demonstrating noncubic behavior. This sample was 7.2 nm and was loaded in 1:1 V/V pentane:isopentane under inert atmosphere.

C. Nonhydrostatic conditions

To avoid nonhydrostatic conditions, it is necessary to have the nanoparticles fully solvated in the hydrostatic medium and dilute enough to prevent aggregation.

As an example of the effects of nonhydrostatic pressure on noble-metal nanoparticles, recently, Guo *et al.*[39] presented results of agglomerated palladium nanocubes showing a distortion mediated by the packing strain of the nanocubes with increasing pressure in a nonhydrostatic pressure medium of silicone oil. They demonstrated that by unraveling the 2D XRD pattern of their nanoparticle into a plot of azimuthal angle vs 2Θ, nonhydrostatic conditions resulted in a waviness of the x-ray diffraction pattern. This method is used in 2D quantitative texture analysis used to evaluate nonhydrostatic stresses.[40,41] We carried out a similar analysis on our x-ray diffraction patterns but did not find any waviness in the unraveled diffraction patterns indicative of nonhydrostatic compression. This is because our particles were well solvated in a hydrostatic medium and were not interacting.

In our experiments, as previously mentioned, we used ethylcyclohexane and a 1:1 by volume mixture of pentane:isopentane as pressure-transmitting fluid. The 1:1 pentane:isopentane mixture does not have a glass transition up to 7 GPa and is hydrostatic up to these pressures.[22,23] Ethylcyclohexane, based on the broadening of ruby fluorescence data acquired in this experiment, is likely only hydrostatic up to a maximum of 4 GPa. Despite the hydrostatic nature of these solvents and full solvation of our nanoparticles, we still observed the distortion behavior. Thereby we rule out nonhydrostaticity in our experiments as the driving cause of the distortion.

It is important to note that nanoparticles that are not agglomerated in the DAC, as in our experiments, will be arranged in many different directions. Therefore, compression along one specific axis, as observed in our experiments, is unlikely. In addition, pressure gradients across the DAC are at most 0.4 GPa as determined from the spatial variations of the ruby fluorescence. A pressure gradient of 0.4 GPa across

the width of the gasket hole (0.3 mm in diameter) is sufficiently small such that a single nanoparticle (a few nanometers in diameter) will not experience any measurable local nonhydrostaticity.

D. Rhombohedral distortion

We recognize that the samples of Ag nanoparticles include a wide variety of particle morphologies, of which only a minority will closely approximate the idealized fcc, icosahedral, and decahedral forms. Each diffraction peak will therefore be a superposition of many peaks from the various lattice planes in these different morphologies. For concreteness and also to help clarify the mechanism that we propose in Sec. IV D, we analyze the d_{111}/d_{200} ratios as if all of the particles were icosahedral, and we further suppose that the curve fitting has identified the strong {111} peak in the icosahedral structure consistent with a rhombohedral crystal structure, which, as previously mentioned, has three times the intensity of the weak {111} peak. The following analysis is therefore not meant to be a precise accounting for the degree of crystalline distortion; rather, it is an estimate of the degree of distortion of a "typical" particle that would be required to explain the results. Thereby we consider these results consistent with grain-boundary-mediated deformation due to the multiply twinned nature of the icosahedral structure of the silver nanoparticles in this intermediate-size range.

We calculate the amount of rhombohedral distortion from the ideal fcc crystal structure via the ratio of the d spacings of the {200} peak to the {111} peak. We represent the rhombohedral deformation as a matrix in reciprocal space, where a is the lattice constant and ϵ is a variable used to represent the amount of rhombohedral distortion as

$$\frac{2\pi}{a}\begin{vmatrix} 1 & 0 & 0 \\ 0 & 1 & 0 \\ 0 & 0 & 1 \end{vmatrix} \rightarrow \frac{2\pi}{a}\begin{vmatrix} 1 & \epsilon & \epsilon \\ \epsilon & 1 & \epsilon \\ \epsilon & \epsilon & 1 \end{vmatrix}. \quad (1)$$

For the {200} direction, we calculate

$$\frac{2\pi}{a}\begin{bmatrix} 1 & \epsilon & \epsilon \\ \epsilon & 1 & \epsilon \\ \epsilon & \epsilon & 1 \end{bmatrix}\begin{bmatrix} 2 \\ 0 \\ 0 \end{bmatrix} = \frac{2\pi}{a}\begin{vmatrix} 2 \\ 2\epsilon \\ 2\epsilon \end{vmatrix}. \quad (2)$$

Thus, the d spacings of the {200}, which is the inverse of the length of this vector, are

$$\frac{1}{d_{\{200\}}} = \frac{2\pi}{a}\sqrt{4 + 8\epsilon^2}. \quad (3)$$

The {111} direction is more complicated to represent because there are eight total reflections: $\pm(111)$, $\pm(\bar{1}11)$, $\pm(1\bar{1}1)$, and $\pm(11\bar{1})$. We are primarily concerned with the position of the most intense reflection which gives the strong {111} reflection. In a rhombohedral distortion, the $\pm(111)$ reflection should be the weaker reflection.[7] We consider the d spacing of the $(1\bar{1}1)$ reflection, whose d spacing is equivalent to the remaining reflections,
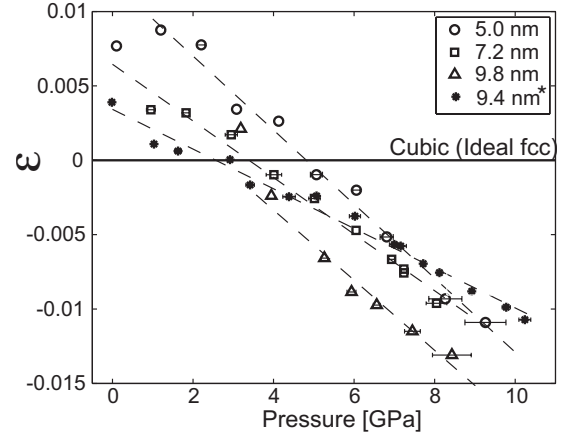

FIG. 8. Degree of rhombohedral distortion, ϵ, as a function of pressure for a variety of nanoparticle samples as calculated in text. Sample labeled with an asterisk was exposed to oxygen during sample loading.

$$(1\bar{1}1) \rightarrow \frac{2\pi}{a}\begin{bmatrix} 1 & \bar{\epsilon} & \epsilon \\ \epsilon & 1 & \epsilon \\ \epsilon & \epsilon & 1 \end{bmatrix}\begin{bmatrix} 1 \\ -1 \\ 1 \end{bmatrix} = \frac{2\pi}{a}\begin{vmatrix} 1 \\ -1 + 2\epsilon \\ 1 \end{vmatrix}, \quad (4)$$

with a corresponding d spacing given by

$$\frac{1}{d_{\{111\}}} = \frac{2\pi}{a}\sqrt{3 - 4\epsilon + 4\epsilon^2}. \quad (5)$$

The ratio of the d spacings of the {200} and the {111} is

$$\frac{d_{\{200\}}}{d_{\{111\}}} = \frac{\sqrt{3 - 4\epsilon + 4\epsilon^2}}{\sqrt{4 + 8\epsilon^2}}. \quad (6)$$

Solving for ϵ gives the amount of distortion from the fcc structure. There are two solutions for ϵ from the solutions of the quadratic formula, but one of those is clearly unphysical since we ascribe ϵ (the amount of distortion) to be small. Figure 8 shows the amount of deviation from cubic symmetry, ϵ, assuming a rhombohedral distortion as a function of pressure.

At low pressures, it becomes increasingly difficult to fit the {200} peaks to extract out the d spacings because at these low pressures, these peaks are broader and run into the tail ends of the {111} peaks. At higher pressures, where d spacings can be fit from the {200} peak more reliably, we see that each size of Ag nanoparticle follows a mostly linear trend in distortion versus pressure. At some pressure that varies with particle size, the amount of distortion returns to a zero value (basically cubic again) and then continues to rhombohedrally distort more in the opposite direction. Error bars are not shown for clarity but are on the order of 0.0008 to 0.001 in ϵ. A line is drawn where $\epsilon=0$; this is where the crystal structure resembles a more ideal fcc.

The slope of the rhombohedral distortion of the sample loaded in air is noticeably different while the others have similar slopes but different intercepts with lower epsilon intercepts for larger particles. As we consider larger particle sizes, we presume that the amount of rhombohedral distor-

tion needed to maintain an icosahedral structure should be less just because more of the atoms are far from the twin boundaries and thus more free to relax toward the bulk fcc form. Also this means that there should be less rhombohedral distortion with increasing pressure, and the return to a cubic nondistorted value should happen at lower pressures. As particle size decreases, there is more rhombohedral distortion and a higher intersection pressure for a crystal structure resembling an ideal cubic structure.

This plot clearly demonstrates that: (i) the trends are statistically significant, (ii) the distortion is real, (iii) the distortion continuously varies with pressure, (iv) the distortion and cubic intercept show size-dependent trends, and (v) the distortion is altered when a sample is exposed to oxidation.

E. Proposed mechanism

The data unambiguously show a departure from cubic symmetry in the ratios of the d spacings. TEM images suggest that the nanoparticles of this study share much of the essential crystallography (i.e., twin pentajunctions and exposed {111} surfaces) with the high-symmetry (icosahedral and decahedral) nearly ideal structures reported by other groups, and thus it is expected that the particles should possess similar crystallographic distortions. For example, each tetrahedron in an icosahedron must, to maintain strain compatibility, compress in the {111} direction normal to its exposed face [Fig. 9(A)].[7] Keeping in mind that this morphology and detailed grain structure vary from one particle to the next, we can expect a statistical distribution of distortion parameters. The icosahedral and decahedral structures thus serve as idealized special cases phenomenologically similar to the particles actually being measured. Let us consider how our observed distortions may arise in such an idealized particle. Since we have found a distortion that is a very strong function of pressure that characteristically resembles a rhombohedral-like distortion, and even reverses in sign at a pressure that varies with nanoparticle size, we propose a mechanism for this transition based on the assumption of a rhombohedral-like distortion and on the bond distribution characteristic of the idealized case of a multiply twinned icosahedral particle.

There are 20 irregular tetrahedral pieces that constitute an ideal icosahedron. The crystallographic configuration possesses a rhombohedral structure that is the result of a uniaxial strain along a [111] direction in the fcc crystal to stabilize the atoms in the icosahedron.[7] Rhombohedral crystallography leads to a bimodal distribution of bond lengths. The packing of the atoms in this structure has been well described by Mackay.[42] To explain the proposed mechanism (detailed below), Fig. 9(B) presents an illustrative tetrahedron of these atomic arrangements and corresponding bonds. Here, only the shorter bonds have been drawn to illustrate the proposed mechanism of compression. In the icosahedral structure, for atoms that are in the {111} planes parallel to the exposed surface, the bonds between in-plane neighbors are longer while the bonds between any two of these planes are shorter. Compressing normal to these planes is therefore more difficult than an in-plane compression as it would force the
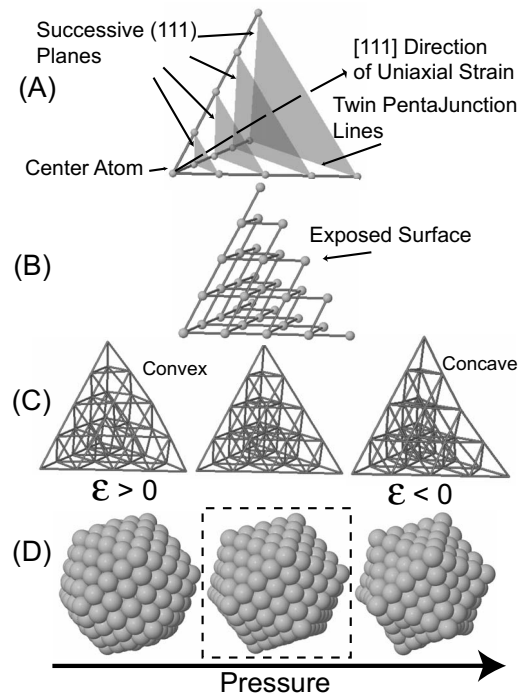

FIG. 9. Illustrative diagram depicting (A) a schematic of a single distorted tetrahedron—1/20th of the icosahedron with only the (111) planes drawn. (B) The same tetrahedron in a ball and stick form with only the short interplanar bonds drawn—the longer intraplanar bonds are removed for clarity. (C) The tetrahedron, now with all bonds shown, with a continuous distortion that would allow the effective average $d_{\{200\}}/d_{\{111\}}$ to vary. (D) The icosahedra resulting from the distortions in (C). A dashed box is drawn around the ideal undistorted icosahedron. ϵ is the degree of rhombohedral distortion described in text. Visualization of these structures was done with JMol (Ref. 43).

shorter bonds to become even shorter. It is far more likely that, as the pressure increases, the longer bonds will be subject to more compression than the shorter bonds.

The tetrahedron's other three {111} faces (the twin boundaries) consist of mostly shorter bonds, while most of the corresponding interplanar bonds are longer. Therefore it should be easier to press these planes closer together than it would be for the planes parallel to the exposed surface. It is these three {111} directions that yield the strong {111} diffraction peak for the rhombohedrally distorted crystal, while the weak {111} peak corresponds to d spacings normal to the exposed face. Since we are assuming that the peak fitting in the data analysis is tracking the strong {111} peak, we would expect the {111} d spacings to show higher compressibility than would be expected for a cubic crystal. This is in fact exactly what we observe. However, symmetry and strain compatibility in the icosahedral structure force the twin planes to remain essentially fixed throughout any such distortion so that the anisotropic compression can only be accommodated by introducing an inhomogeneous strain within each grain. Recall Ref. 5, which shows that at zero pressure such a distortion produces a convex curvature of the exposed faces. We have found, by simulating such a distortion in a model [left column of Figs. 9(C) and 9(D); distortion exag-

gerated for clarity], that the resulting bond-length distribution corresponds to a positive value of our ϵ parameter. We then consider what must happen to this inhomogeneous strain as the pressure is increased, assuming (consistent with our measurements showing that the strong {111} peak is more compressible than expected) that the longer bonds will compress much more than the shorter bonds. This distortion corresponds to a gradual reduction, and eventually a reversal, in the curvature of the outer faces [middle and right columns of Figs. 9(C) and 9(D)] so that our measured ϵ parameter reverses in sign. We suggest, from the behavior of the x-ray diffraction patterns with decreasing pressure, that this presumed transition from convex to concave is elastic and reversible.

As alluded to earlier, with increasing nanoparticle size, more atomic layers are added to the icosahedral structure. Thus more of the atoms are in relatively bulklike regions far from the twin boundaries. The amount of uniaxial strain each atom takes up in the rhombohedral configuration becomes less; thus, the degree of rhombohedral distortion for bigger particles should be less thereby explaining the size-dependent trend observed in the data.

F. Lack of distortion in platinum fcc nanoparticles

It has been demonstrated that multiply twinned platinum nanoparticles transform into cuboctahedral-shaped single-crystal fcc nanoparticles with annealing and that platinum, unlike silver, often possesses fcc structure down to sizes as small as 10 Å.[44,45] Therefore, as a demonstration of a sample lacking a grain-boundary-mediated distortion that may become more evident with pressure, platinum serves as an ideal candidate and proves to be a useful control to rule out artifacts of the measurement.

Figure 6 presented the ratio of the Pt $d_{\{200\}}/d_{\{111\}}$ from experimental x-ray diffraction peaks as a function of pressure. The data do not show the same noncubic distortion trend with pressure as was observed for Ag nanoparticles. This provides evidence that the distortion behavior of Ag nanoparticles detected in these studies is the result of the multiply twinned pentagonal nature of the silver nanoparticles. This also serves as a useful test of our proposed mechanism based on the multiply twinned nature of the silver nanoparticles which is lacking in platinum nanoparticles.

V. CONCLUSIONS

This study clearly demonstrates that silver nanoparticles in the size range of 5–10 nm undergo a reversible noncubic distortion with pressure. The trends are statistically significant, the distortion is real, the distortion continuously varies with pressure, the distortion is size dependent, and the distortion is altered when a sample is exposed to oxidation.

We posed the question: what happens to the internal strain of multiply twinned structures if one introduces an external stress? In the case of silver nanoparticles, the predominant ambient structure is multiply twinned and ideally icosahedral. The ambient strain is uniaxial along a [111] direction resulting in a rhombohedral distortion. The Ih silver nanoparticles have a convex appearance. Our results suggest that addition of pressure affects the nanoparticle such that the structure starts to bow more inward in a concave manner, becoming less convex, through a further rhombohedral distortion thereby altering the appearance of the icosahedron with pressure.

This study shows that cubic symmetry can be broken in fcc noble-metal nanoparticles, e.g., through surface phenomena and twin pentajunctions, yielding rhombohedral distortions even at zero pressure that show pressure-dependent and size-dependent behaviors. The low energy per unit area of {111} surfaces and of coherent twin boundaries is able to compete with the energy per volume of the crystallographic distortion when dealing with small particles and grains under pressure.

Our results raise the question: is this an example of a really general phenomenon or would this happen in other materials with similar and different grain structures such as Dh gold or Ih palladium? Future measurements on other similar multiply twinned particles would help answer this question. Further calculations would also help elucidate the nature of this distortion in silver nanoparticles under pressure.

*alivis@berkeley.edu

[1] C. L. Johnson, E. Snoeck, M. Ezcurdia, B. Rodríguez-González, I. Pastoriza-Santos, L. M. Liz-Marzán, and M. J. Hÿtch, Nature Mater. **7**, 120 (2008).

[2] V. G. Gryaznov, J. Heydenreich, A. M. Kaprelov, S. A. Nepijko, A. E. Romanov, and J. Urban, Cryst. Res. Technol. **34**, 1091 (1999).

[3] Y. Tang and M. Ouyang, Nature Mater. **6**, 754 (2007).

[4] C. Mohr, H. Hofmeister, and P. Claus, J. Catal. **213**, 86 (2003).

[5] D. Reinhard, B. D. Hall, D. Ugarte, and R. Monot, Phys. Rev. B **55**, 7868 (1997).

[6] L. D. Marks, Rep. Prog. Phys. **57**, 603 (1994).

[7] C. Y. Yang, J. Cryst. Growth **47**, 274 (1979).

[8] V. G. Gryaznov and L. I. Trusov, Prog. Mater. Sci. **37**, 289

(1993).

[9] F. Silly and M. R. Castell, Appl. Phys. Lett. **87**, 213107 (2005).

[10] X. Xing, R. M. Danell, I. L. Garzón, K. Michaelian, M. N. Blom, M. M. Burns, and J. H. Parks, Phys. Rev. B **72**, 081405(R) (2005).

[11] B. D. Hall, M. Fluëli, R. Monot, and J.-P. Borel, Phys. Rev. B **43**, 3906 (1991).

[12] G. C. Kennedy and R. N. Keeler, *American Institute of Physics Handbook*, 3rd ed. (McGraw-Hill, New York, 1972), Sec. 4, p. 101.

[13] Y. Akahama, H. Kawamura, and A. K. Singh, J. Appl. Phys. **95**, 4767 (2004).

[14] Q. F. Gu, G. Krauss, F. Gramm, A. Cervellino, and W. Steurer, Phys. Rev. Lett. **100**, 045502 (2008).

[15] K. S. Suslick, M. Fang, and T. Hyeon, J. Am. Chem. Soc. **118**, 11960 (1996).

[16] M. Green, Chem. Commun. (Cambridge) **2005**, 3002.

[17] Y. Yin, C. Erdonmez, S. Aloni, and A. P. Alivisatos, J. Am. Chem. Soc. **128**, 12671 (2006).

[18] N. S. Sobal, U. Ebels, H. Möhwald, and M. Giersig, J. Phys. Chem. B **107**, 7351 (2003).

[19] F. Baletto and R. Ferrando, Rev. Mod. Phys. **77**, 371 (2005).

[20] M. Kunz, A. A. MacDowell, Wendel A. Caldwell, D. Cambie, R. S. Celestre, E. E. Domning, R. M. Duarte, A. E. Gleason, J. M. Glossinger, N. Kelez, D. W. Plate, T. Yu, J. M. Zaug, H. A. Padmore, R. Jeanloz, A. P. Alivisatos, and S. M. Clark, J. Synchrotron Radiat. **12**, 650 (2005).

[21] A. P. Hammersley, ESRF Internal Report No. ESRF98HA01T, FIT2D, 1998 (unpublished).

[22] W. F. Oliver, C. A. Herbst, and G. H. Wolf, J. Non-Cryst. Solids **131-133**, 84 (1991).

[23] G. J. Piermarini, S. Block, and J. D. Barnett, J. Appl. Phys. **44**, 5377 (1973).

[24] J. N. Wickham, A. B. Herhold, and A. P. Alivisatos, Phys. Rev. Lett. **84**, 923 (2000).

[25] K. Jacobs, D. Zaziski, E. C. Scher, A. B. Herhold, and A. P. Alivisatos, Science **293**, 1804 (2001).

[26] K. Jacobs, D. Zaziski, E. C. Scher, A. B. Herhold, and A. P. Alivisatos, J. Phys. Chem. B **106**, 3759 (2002).

[27] G. J. Piermarini, S. Block, J. D. Barnett, and R. A. Forman, J. Appl. Phys. **46**, 2774 (1975).

[28] H. K. Mao, P. M. Bell, J. W. Shaner, and D. J. Steinberg, J. Appl. Phys. **49**, 3276 (1978).

[29] P. Vinet, J. H. Rose, J. Ferrante, and J. R. Smith, J. Phys.: Condens. Matter **1**, 1941 (1989).

[30] R. F. S. Hearmon, Rev. Mod. Phys. **18**, 409 (1946).

[31] R. Bacon and C. S. Smith, Acta Metall. **4**, 337 (1956).

[32] J. R. Neighbours and G. A. Alers, Phys. Rev. **111**, 707 (1958).

[33] K. N. Khanna, Solid State Commun. **29**, 801 (1979).

[34] P. Mahazzabi, J. Phys. Chem. **46**, 147 (1985).

[35] A. Wolfenden and M. R. Harmouche, J. Mater. Sci. **28**, 1015 (1993).

[36] J. F. Nye, *Physical Properties of Crystals* (Clarendon, Oxford, UK, 1957), pp. 144–145.

[37] W. M. Moore and P. J. Codella, J. Phys. Chem. **92**, 4421 (1988).

[38] S. Krüger, S. Vent, F. Nortemann, M. Staufer, and N. Rösch, J. Chem. Phys. **115**, 2082 (2001).

[39] Q. Guo, Y. Zhao, W. L. Mao, Z. Wang, Y. Xiong, and Y. Xia, Nano Lett. **8**, 972 (2008).

[40] L. Miyagi, S. Merkel, T. Yagi, N. Sata, Y. Ohishi, and H.-R. Wenk, J. Phys.: Condens. Matter **18**, S995 (2006).

[41] G. Ischia, H.-R. Wenk, L. Lutterotti, and F. Berberich, J. Appl. Crystallogr. **38**, 377 (2005).

[42] A. L. Mackay, Acta Crystallogr. **15**, 916 (1962).

[43] http://www.jmol.org

[44] C. Solliard and M. Flueli, Surf. Sci. **156**, 487 (1985).

[45] B. Raoult, J. Farges, M. F. De Feraudy, and G. Torchet, Philos. Mag. B **60**, 881 (1989).